IEEE Access
Multidisciplinary ⋮ Rapid Review ⋮ Open Access Journal

Received 13 May 2023, accepted 24 May 2023, date of publication 29 May 2023, date of current version 7 June 2023.

Digital Object Identifier 10.1109/ACCESS.2023.3280856

RESEARCH ARTICLE

Design and Analysis of an Asymmetric Spoke and Delta-Shape Interior Permanent Magnet Synchronous Machine

NIAZ MUHAMMAD[1], FAISAL KHAN[1], (Senior Member, IEEE), BASHARAT ULLAH[1], (Member, IEEE), SAIRA TARIQ[1], AND AHMAD H. MILYANI[2,3]

[1]Department of Electrical and Computer Engineering, COMSATS University Islamabad, Abbottabad Campus, Abbottabad 22060, Pakistan
[2]Department of Electrical and Computer Engineering, King Abdulaziz University, Jeddah 21589, Saudi Arabia
[3]Center of Research Excellence in Renewable Energy and Power Systems, King Abdulaziz University, Jeddah 21589, Saudi Arabia

Corresponding author: Niaz Muhammad (niazmuhammad724@gmail.com)

ABSTRACT This paper proposes a design of an asymmetric spoke and delta-shape interior permanent magnet (AIPM-P) synchronous machine for electric vehicles that use the magnetic-field-shifting (MFS) technique to improve the average torque and reduce torque ripples. The asymmetry of the AIPM-P is due to the asymmetric rotor structure, asymmetric permanent magnet (PM) placement, and asymmetric flux barriers (AFB). Due to this asymmetry, the MFS is utilized, which decreases the current angle difference between the peak PM torque (T_{PM}) and reluctance torque (T_r) components. In the delta-shape, the bar magnet helps reduce the d-axis inductance, which helps in increasing the reluctance torque, ultimately increasing synthetic torque. Furthermore, the combination of delta-shape and spoke shape PM makes the novel hybrid layer structure that improves the average torque. The proposed AIPM-P is then compared with the conventional designs in the literature having the same stator and rotor radius, with a 4-pole and 24-slot combination. The open circuit, on-load characteristics, efficiency, copper, and iron loss maps of the proposed and conventional designs are investigated and compared. Compared to the conventional designs, the proposed AIPM-P synchronous machine has high efficiency and a good torque profile, which is suitable for EV applications.

INDEX TERMS Asymmetric rotor, asymmetric interior PM cavity, delta and spoke type PM, magnetic-field-shifting.

I. INTRODUCTION

Permanent magnet (PM) machines are primarily used in industrial and electric vehicle (EV) applications because they have high power density, torque density, efficiency, power factor, and constant power speed range (CPSR) [1]. Due to these advantages, it is more applicable for EVs and environmentally friendly. In PM machines, different PM types are used for the performance criteria, such as a rare-earth magnet (NdFeB) and a ferrite magnet [2]. The more suitable interest for these types of machines has a rare-earth magnet that has a good flux linkage power [3]. Nowadays, researchers are also involved in employing inexpensive PM materials like ferrite and Al-Ni-Co in multilayer IPM machines to reduce the need for rare-earth materials, but the structure of the machine becomes complex due to the multilayer. For applications requiring high torque density, a synchronous motor with ferrite magnets is recommended in [4].

According to the PM placement, the PMs machine's rotor is divided into two categories, surface mounted permanent magnet (SPM) and interior permanent magnet (IPM) motor rotors [4]. In SPM, the PMs are attached to the outer side of the rotor while in IPM, the PMs are buried inside the rotor. SPM motors' mechanical strength is lower than that

The associate editor coordinating the review of this manuscript and approving it for publication was R. K. Saket.

TABLE 1. Structure wise differences in the topologies presented in literature.

Ref	Design Topology	PMs Configuration	Flux barrier type	Rotor structure
[9]	Symmetrical	Delta-shape, double V-shape and V-shape	Symmetrical	Symmetrical
[13]	Asymmetrical	Spoke and V-shape	Asymmetrical	Asymmetrical
[14]	Symmetrical	U and delta shape	Symmetrical	Symmetrical
[16]	Symmetrical	Spoke-type, bar-type, U-type, and V-type	Symmetrical	Symmetrical
[19]	Symmetrical	Spoke-type	Symmetrical	Symmetrical
[20]	Symmetrical	Spoke-type	No extra barrier	Symmetrical
[21]	Asymmetrical	V-shape	Asymmetrical	Asymmetrical
[22]	Symmetrical	Y-shape	Symmetrical	Symmetrical
Proposed design				
AIPM-P	Asymmetrical	Spoke and delta-shape	Asymmetrical	Asymmetrical

of an IPM motor since the magnets are fixed to the rotor surface's outside. IPM motors are adaptable to different EVs because of their magnetic saliency, allowing them to create torque by using both the motor's magnetic and reluctance torque components. In accordance with all research, the IPM motors have become popular driving motors for EVs such as the Lucid, Rimac Nevera, Camry, leaf, Honda accord, GM ChevyBolt, Mitsubishi outlander, Renault Zoe, Audi e-Tron, Porsche Taycan, Tesla model, Toyota Prius, etc. [5], [6], [7], [8], [9], [10], [11].

Many IPM rotor structures have been reported in the literature [12], [13] and used in industry because the performance of IPM machines greatly depends on the rotor topologies, which are characterized by the PM placement and rotor core geometry, including the design of the PM placement cavity, iron bridges, and barriers. The most often used topologies include one and one-half-layers configurations, such as spoke-PMs, V- and flattened form IPMs, and assorted double-layers delta designs because of their superior performance and simplicity in manufacturing. These topologies, together with a U-type structure, are intended for use in electric vehicle applications, and the electromagnetic performances of these topologies are compared. However, these topologies are complex designs based on manufacturing when a detailed performance is investigated [1]. At the same time, [12] reports a comparison of the V-type, U-type, flattened form, and double-layer V and U-type topologies, both comparisons show that the machines with a V-shape design may provide the highest torque density, but the contribution of torque ripples is not considered. The Y-shaped rotor topology for IPM machines is presented in [13], using a 12-slot/10-pole combination and three-phase concentrated winding. The Y-shaped IPM machines have the maximum torque density and lower torque ripples compared to V-shaped and spoke-type machines, but the air gap harmonics occur due to the concentrated winding.

For innovative IPM rotor topologies, increasing torque density without the utilization of high PM volume is still desirable for enhancing machine efficiency. To do this, hybrid rotor designs have received extensive research for enhancing reluctance torque owing to high saliency. Authors in [14] compare IPM machines with different layers of PMs, which enhance the average torque, but multi-layer PM rotor topologies make optimization design challenging and provide difficulties for PM manufacturing. A spoke-type PM, which has 12-slot and 10-pole, and detachable rotor laminae, are used in the study [15] to propose an IPM machine with a high-power density. Several IPM rotor topologies are documented in the literature, including bar, V-shape, delta, and double V-shape PM placement in the rotor [16] and [17], as well as hybrid or multi-layer designs [14], and the spoke-PM placement topologies [18], [19]. Out of these concepts, the spoke-shape IPM motors are attractive options for certain applications because of their simple rotor structure of a piece of PM, which is placed to concentrate each pole-potential flux, low cost, and simplicity of quick manufacturing with automated PM assembly [19] through [20]. Although the reduction of torque ripples occurs due to the spoke PMs, but the torque density is also reduced. Optimization of geometry parameters also plays an important role in improving the performance of machine. Several multi-objective optimization technique were proposed in literature for the said purpure. In [28], a system-level design optimization method based on the actual operating environment is proposed. In [29] and [30] multi-objective optimization based on sequential subspace optimization and sequential Taguchi method was proposed, respectively. These researches mainly focus on the comprehensive optimization of motor efficiency and electromagnetic performance by using different multi-objective optimization methods.

The current generation of IPM machines features symmetrical rotor constructions with current angles generally 45 electrical degrees (ED) for the maximum PM and reluctance torque components, which reduces the utilization ratios of both portions in the maximum resultant torque. Utilizing the MFS effect, a unique asymmetric rotor construction closely changes the peak points of the PM and reluctance torque components, increasing the torque while utilizing the same volume of PM [21]. In [22], different design structures are explained, which are symmetric and asymmetric to rotor core structure and PMs cavity configurations. In these designs, the asymmetric design torque profile is better than the symmetrical one. Mainly there are four categorization methods of AIPM machine topologies explained. IPM with a V-type magnet configuration [23] introduces an asymmetric flux barrier (AFB) that increases the average torque. A mix of V-type magnet configuration and spoke-type PMs with

AFB are introduced for torque enhancement. This clearly shows the average torque increase using the magnetic field shifting effect phenomenon [24]. Some other relevant studies are reported in [25]. The relevant literature is summarized in Table 1, which presents the structure wise differences in the topologies mentioned in this paper.

To overcome the aforementioned flaws in a different state of the art, this paper proposes an asymmetric delta-shape and spoke-shape permanent magnet synchronous machine which has the asymmetric rotor and PM structures with AFB that enhance the torque and decrease the torque ripples. The delta-shape PMs contribute to enhancing the torque, and spoke-type reduces torque ripples. This paper has the following sections: Section II explains the proposed design of AIPM-P, AIPM-I, and AIPM-II, shown in Fig. 1, the concept of MFS techniques and parametric optimization. Section III compares the three designs' electromagnetic (EM) performance, power vs. speed, and torque vs. speed characteristics and the comparison of the efficiency mapping. At last, Section IV is the conclusion of this paper.

II. MACHINE DESIGNS

A. DIFFERENT MACHINE DESIGNS

The proposed design of asymmetric spoke and mixed delta-shape PM cavities with additional asymmetric flux barriers is illustrated in Fig. 1a. The two AFB are attached to the right sides of delta-shape PMs and at the left sides of spoke-type PMs, close to the rotor surface on each pole side, which is compared with conventional (AIPM-I) asymmetric rotor topology with a one and one-half layer combined spoke-PM and V-shape structure is shown in Fig. 1b. The angle changes between the axis of the delta and spoke PMs cavities, as well as the location and size of the AFB, highlight the asymmetry of the two structures. These features lead to an uneven distribution in the cavity design and PM configuration of the AIPM, which produces the MFS effect for torque enhancement. Also, another structure (AIPM-II) for the benchmark is illustrated in Fig. 1c, which has a hybrid layer asymmetric PM configuration in an asymmetric rotor structure. So this design also uses the magnetic field shifting technique to improve torque. As with AIPM-P, AIPM-I, and AIPM-II, all three designs use the same rotor and stator diameter. The stator has identical 24-slot and 4-pole distributed windings for all presented designs, depicted in Fig. 1d. The magnetization pattern of all the PM is given in Fig. 1.

Fig. 2 indicates the rotor geometrical model for the proposed AIPM-P. The AIPM-P q-axis stays at a 90° angle from the d-axis, whereas the d-axis is situated at the middle axis among neighbouring spoke-shape PMs. The electrical angle among the central axis of the spoke-PMs and delta-shape PMs distinguishes the location of the delta-shape PMs structure called θ_{ds} in four poles, which shows the asymmetry of the delta-shape PMs configuration. β_{ds} is the asymmetry factor for the delta-shape PMs in AIPM-P, which is given below:

$$\beta_{ds} = \frac{4p\theta_{ds}}{360} \tag{1}$$

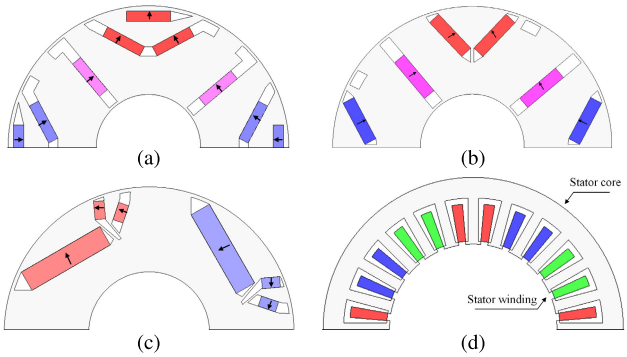

FIGURE 1. Different designs (a) AIPM-P (b) Benchmark AIPM-I (c) Hybrid layer AIPM-II, (d) 24-slot stator.

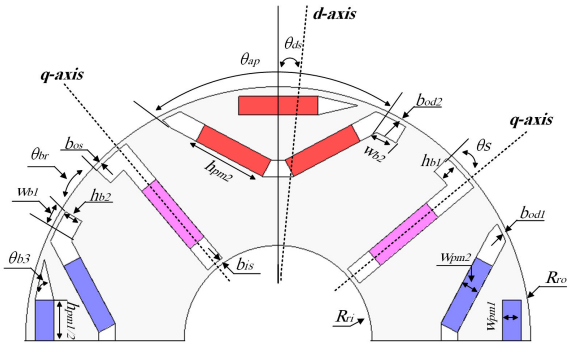

FIGURE 2. Geometrical model of the proposed AIPM-P design and certain key design parameters.

The flux barrier widths w_{b1} and w_{b2} represent the delta-shape barriers, while the h_{b2} is the thickness of the delta-shape barriers, which are connected to the delta-shape PMs structures, h_{b1} is the thickness of the spoke barriers which control the leakage flux of the proposed model, also different layers of the PMs used in the proposed model just like the upper magnet of the delta-shape which has a flux barrier for enhancing the average torque. Concerning the conventional design AIPM-I, the proposed design has 2-layers of the proposed AIPM-P. The proposed AIPM-P uses the same volume of PMs as AIPM-I and AIPM-II with an asymmetric rotor construction to take advantage of the MFS effect and improve average torque. In addition, the proposed AIPM-P and AIPM-I only require four and three pieces of PMs respectively, thus there is not a significant increase in prices or difficulties in manufacturing. Some other dimensions are b_{od1}, b_{od2}, b_{os}, and b_{is}, which show the thickness of the iron bridges connected with the delta-shape PMs, spoke-type PMs, and flux barriers, respectively, w_{pm1} and w_{pm2} are the widths of the spoke and delta-shape PMs. There are some other parameters which are θ_{ap}, θ_{b3} also affect the torque components, θ_{b3} is the barrier angle of the upper magnet of the delta which reduces the leakage flux. θ_{ap} for the proposed design AIPM-P is 124°, while 87° for the conventional design AIPM-I dramatically enhances the average torque.

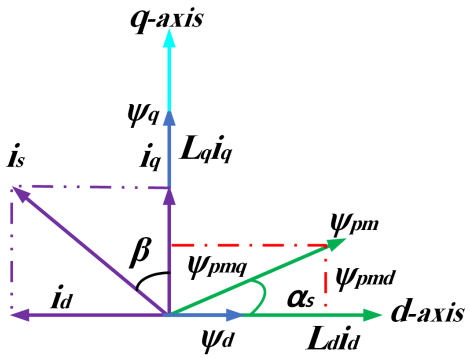

FIGURE 3. AIPM d-axis and q-axis phasor diagram.

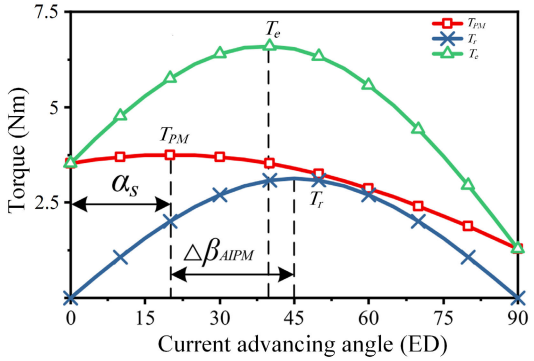

FIGURE 4. Torque segregation of AIPM.

B. CONCEPT OF MFS TECHNIQUE FOR TORQUE ENHANCEMENT

The enhancement of average torque is due to the utilization of the MFS effect phenomenon. To explain the MFS phenomenon take a basic analytical model for a general AIPM machine without considering the magnetic saturation and cross-magnetization. Fig. 3 shows the different terms used for PMs flux linkages, stator current, and flux linkages. In this vector diagram, the i_d and i_q are the d-axis, q-axis and the stator phasor current. While Ψ_d and Ψ_q are the q-axis and d-axis flux linkages which are shown in Eq. (3), (4), Ψ_{pm}, Ψ_{pmd} and Ψ_{pmq} are the PMs flux linkages and its d-axis and q-axes components. While α_s is the asymmetric angle of the AIPM machine and β is the current angle shown in Eq. (2).

$$\beta = tan^{-1}\left(\frac{i_d}{i_q}\right) \tag{2}$$

$$\Psi_d = \Psi_{pmd} - L_d i_d = \Psi_{pm} cos\alpha_s - L_d i_s sin\beta \tag{3}$$

$$\Psi_q = \Psi_{pmq} + L_q i_q = \Psi_{pm} sin\alpha_s - L_q i_s cos\beta \tag{4}$$

The general equation of the torque for the IPM machine is given in Eq. (5).

$$T_e = \frac{m}{2}p(\Psi_d i_d + \Psi_q i_q) = \frac{3}{2}p\Psi_{pm} i_s cos(\beta - \alpha_s) + \frac{3}{2}p(L_q - L_d)i_s^2 sin2\beta \tag{5}$$

TABLE 2. Main design parameter of all three topologies.

Symbol	Units	AIPM-P	AIPM-I	AIPM-II
Air gap, δ	mm	1		
Pole pairs	-	2		
N	-	60		
N_s	-	24		
R_{os}	mm	50		
R_{ri}	mm	10		
R_{ro}	mm	26.9		
PM Volume	mm^3	12960		12600
B_r	T	1.23		
W_{pm1}	mm	2	2.4	3.5, 1.75
W_{pm2}	mm	2	2.4	15, 3
h_{pm1}	mm	8	9	-
h_{pm2}	mm	8.4	-	-
b_{od1}	mm	0.5	0.5	-
b_{od2}	mm	0.5	-	-
b_{is}	mm	0.5	-	-
b_{os}	mm	0.5	-	-
W_{b1}	mm	3.57	-	-
W_{b2}	mm	2.37	-	-
h_{b1}	mm	2	-	-
h_{b2}	mm	2	-	-
θ_{ap}	ED	124	87	-
θ_{br}	-	0.15	-	-
θ_{b3}	-	0.01	-	-
θ_s	-	0.5	-	-

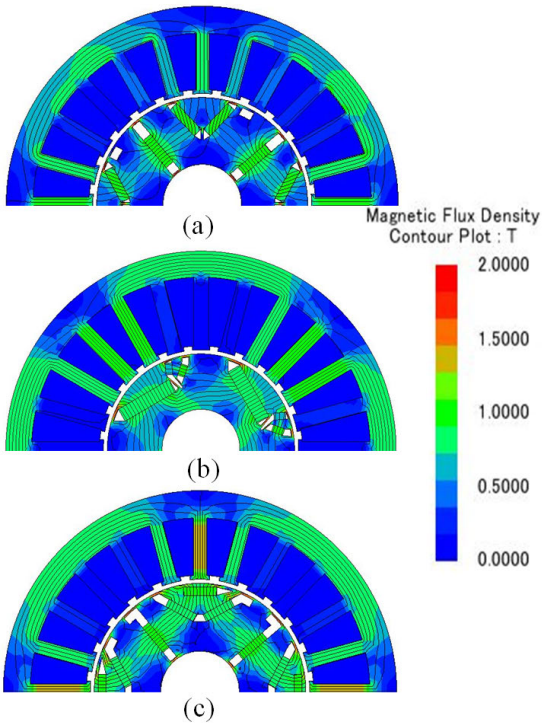

FIGURE 5. Comparison of flux lines distribution at no-load of the three designs (a) AIPM-I, (b) AIPM-II, (c) AIPM-P.

where T_e is the total torque, $m = 3$ is the phase number, and p is the number of poles for general IPM.

$$T_m = \frac{3}{2}p\Psi_{pm} i_s cos(\beta - \alpha_s) \tag{6}$$

$$T_r = \frac{3}{2}p(L_q - L_d)i_s^2 sin2\beta \tag{7}$$

$$T_e = T_m + T_r \tag{8}$$

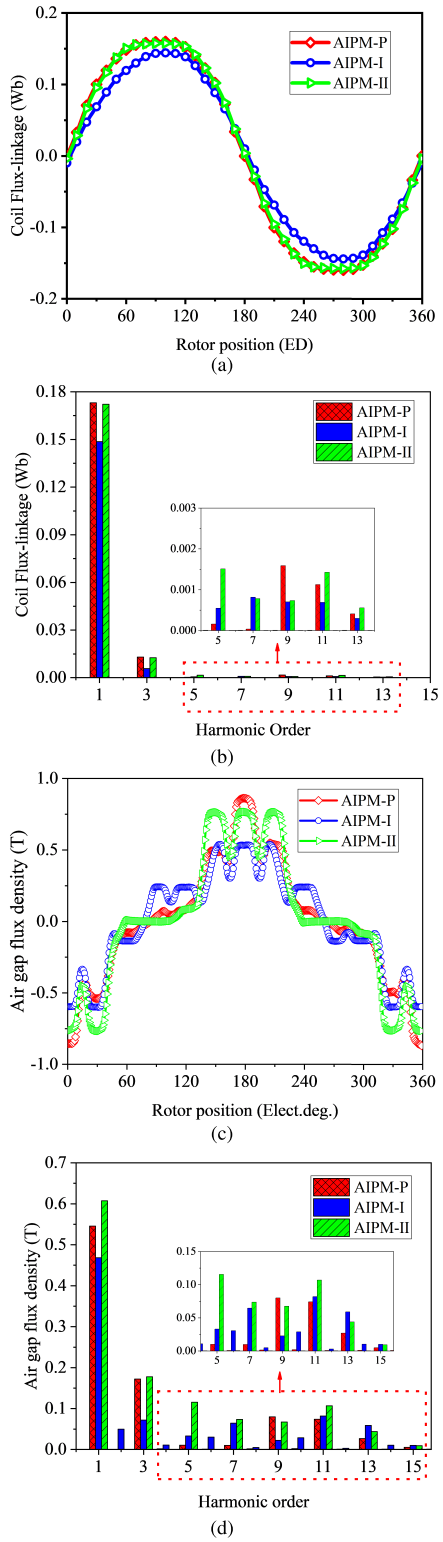

FIGURE 6. Comparison of no-load coil flux linkages and air gap flux densities (a) Coil flux-linkage waveform (b) Spectra (c) Air gap flux-densities waveform (d) Harmonic spectra.

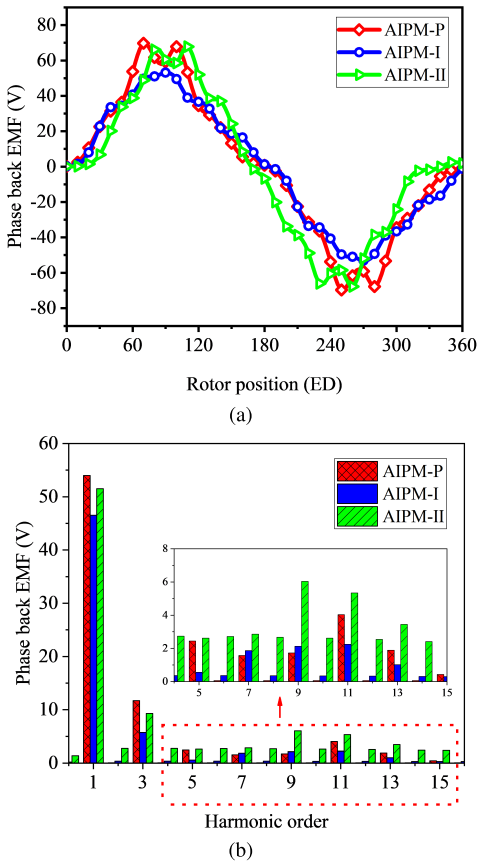

FIGURE 7. No-load Phase-A back-EMFs comparison. (a) Waveforms, (b) Spectra.

TABLE 3. Comparison of the proposed design with conventional designs.

Parameter	[13]	[26]	[27]	AIPM-P
Air gap, δ (mm)	1	1	0.6	1
Number of slots, N_s	24	24	12	24
Number of turns, N	60			
Stack length (mm)	50			
PM type	N38			
Excitation current (A)	10			
R_{os} (mm)	50			
R_{ro} (mm)	26.9	24	26.9	26.9
PM volume (mm^3)	12960	12600	13280	12960
Rated speed (rpm)	1500	1500	750	1500
Average torque (Nm)	6.41	6.34	7.95	6.78
Torque ripples (%)	20	18	5.1	16
T_{PM*} (kNm/mm^3)	0.4946	0.5032	0.5986	0.5486
Efficiency (%)	94	94	94.6	95.41

*Torque per PM volume

Eq. (8) shows the equivalent torque (T_e) which is the sum of reluctance torque (T_r) and PM torque (T_{PM}). The T_{PM} torque is produced from the PM flux interaction with an armature rotating magnetic field, and the T_r is due to the rotor saliency.

$$\Delta\beta_{AIPM} = \frac{\pi}{4} - \alpha_s \tag{9}$$

Theoretically, the advanced current angle difference ($\Delta\beta_{AIPM} = 45 - \alpha_s$) of IPM machines is normally 45 electrical degrees (ED) because α_s for IPM machine is zero while the current angle difference of AIPM between the T_r and T_{PM} becomes closer together due to the MFS effect with the positive value of α_s which is the asymmetry factor of

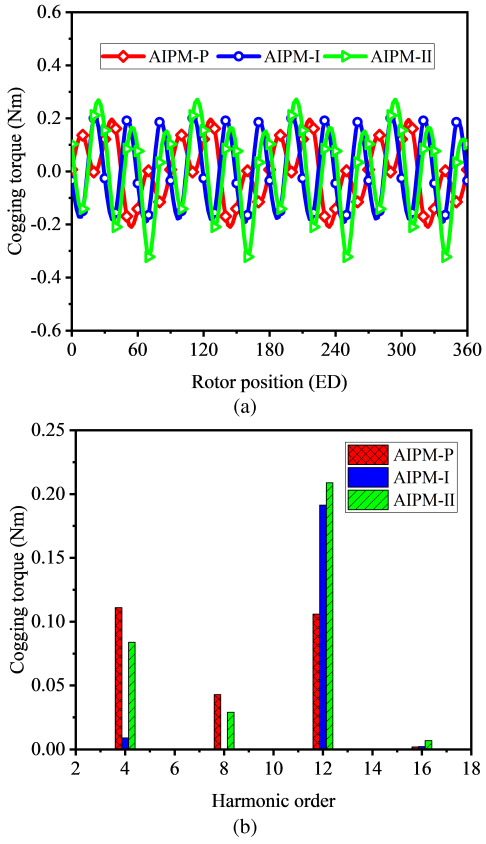

FIGURE 8. Cogging torque. (a) Wave shape, (b) harmonic spectra.

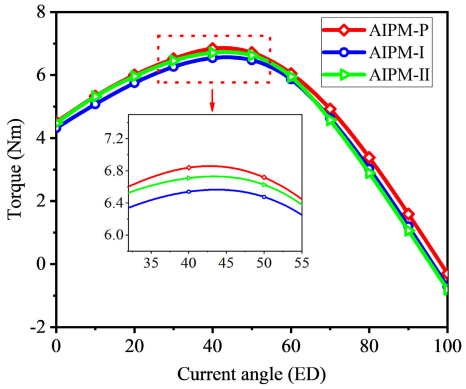

FIGURE 9. Torques versus current angles of all the presented topologies at 1500 rpm and $I_{max} = 10A$.

the AIPM synchronous machine shown in Eq. (9). In this way, when the current angle difference decreases, the average torque of the AIPM increases due to the peak point of PM torques, and reluctance torques are shifted to be closer as shown in Fig. 4.

C. PARAMETRIC OPTIMIZATION

Additionally, the parametric optimization procedure is used to refine the angle between V-shape PMs (θ_{ap}), the position of bar magnet and the position of asymmetric flux barrier

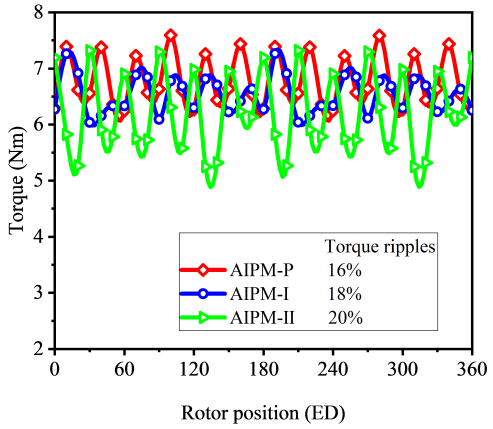

FIGURE 10. Instantaneous torque curve at 1500 rpm at a current of 10A.

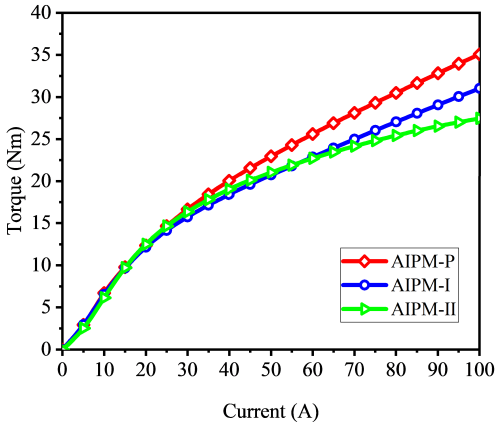

FIGURE 11. Torques vs current (A) waveform comparison at 1500 rpm.

parameters with its main objective being to maximize the average torque. Table 2 provides a summary of the essential design parameters for the three topologies ultimate optimum designs, and Fig. 5 shows the distributions of the open-circuit field and flux lines for the best structures. It illustrates how the right of the delta-shaped cavity in the regular AIPM-P optimum solution is connected to the flux barrier, while the left side of the barrier cavity is shifted to be nearer to the spoke-shaped PMs. Both characteristics are in line with the findings of the parametric analysis. In section III, the EM of all three topologies AIPM-P, AIPM-I, and AIPM-II to conduct a more in-depth analysis are compared.

III. COMPARISON OF ELECTROMAGNETIC PERFORMANCES

A. NO-LOAD ANALYSIS

Fig. 6 shows the comparison of no-load coil flux linkages wave shape and harmonic spectra of the three designs. Besides the open circuit air gap flux density wave shape, spectra, and essential components of the three asymmetrical machines, the air gap flux density of the presented designs are almost the same, although the AIPM-P, AIPM-I, and

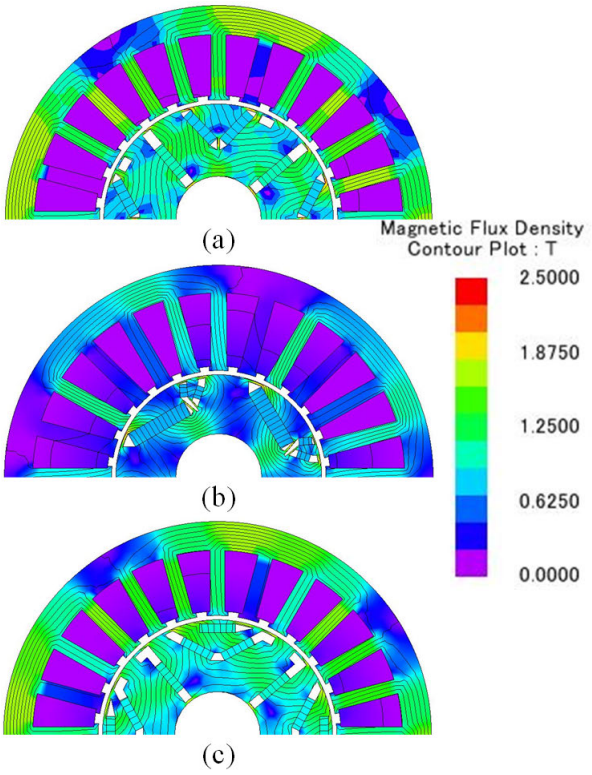

FIGURE 12. Display of load magnetic flux density and flux line linkages (a) AIPM-I, (b) AIPM-II, (c) AIPM-P.

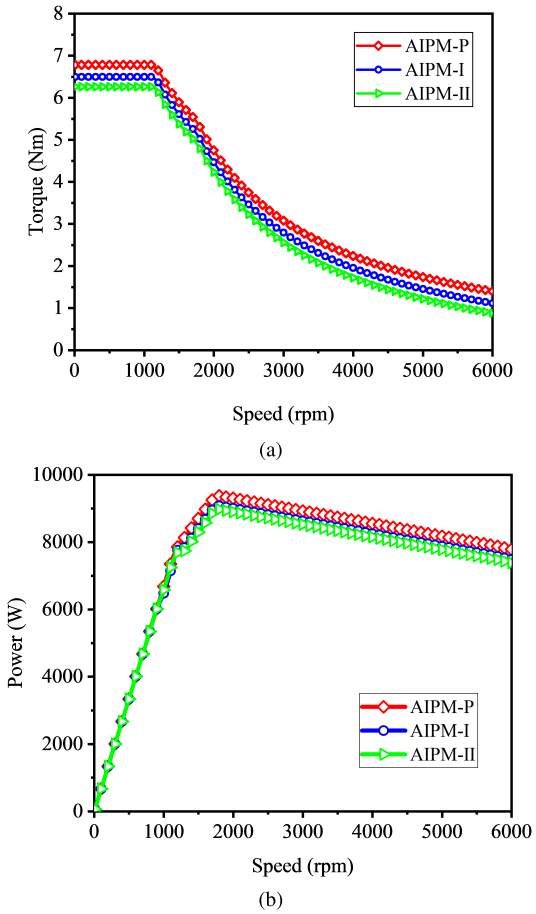

FIGURE 13. Comparison of constant power speed range characteristics at V_{dc} 120V, current amplitude 10A, (a) Torque vs Speed waveform, (b) Power vs Speed waveform.

AIPM-II have relatively the same results of harmonic distortion because the higher value of the air gap flux density of the AIPM illustrates the MFS effect at the no-load condition. While Fig. 7 shows the comparison of no-load back electromotive force (EMF) waveforms and spectra of Phase-A windings in three asymmetrical designs. The difference in the back-EMF of the proposed AIPM-P, AIPM-I, and AIPM-II is less compared to its effect, but the proposed model has a more significant EMF than the other two conventional designs. The overall harmonic distortion of the back-EMF is without the third harmonic distortion, which is negligible in Y-connection windings in three topologies. Fig. 8a compares the cogging torque waveform of the three designs, showing that the proposed design has lower cogging torque than the other two asymmetrical topologies. The spectra of the cogging torque presented in Fig. 8b also reveal that the 12th harmonic is the dominant harmonic in all three asymmetrical.

B. LOAD ANALYSIS

The comparison of the EM performances of the three topologies is given in Table 3, and the torque-current angle of the presented topologies at the current of 10A and 1500 rpm is shown in Fig. 9. The proposed design of asymmetric spoke-type and mixed-delta shape achieves higher torque than the other two asymmetrical machine topologies AIPM-I and AIPM-II, due to the upper flat shape PM flux linkages of the delta is higher than the V-shape PMs because of the decreases in d-axis inductance.

Additionally, it can be shown that when compared with the asymmetrical topologies AIPM-I and AIPM-II, the AIPM-P achieves the maximum average torque, which is 6.78 Nm at a little greater phase angle. Besides, the torque of the AIPM-P hits '0' at the current angle of roughly 95 ED, whereas the average torques of the two asymmetrical topologies do so at 90 ED, which suggests that the MFS effect has an impact on torque performance, which always shows that this effect enhances the average torque of the AIPM-P machine.

Thus, it is shown that the hybrid layer structure and magnetic field shifting effect both contribute to improving the average torque of AIPM-P over the spoke and mixed V-shape AIPM-I, and these features can show effectively increase the average torque of the proposed topology, which are investigated by finite element analysis. Additionally, it is proven that the proposed AIPM-P PMs structure demonstrates MFS effects that are comparable to those of traditional multi-layer structures, particularly concerning the improvement of average torque. In summary, the proposed AIPM-P architecture is a strong contender for IPM machines for applications requiring large torque densities.

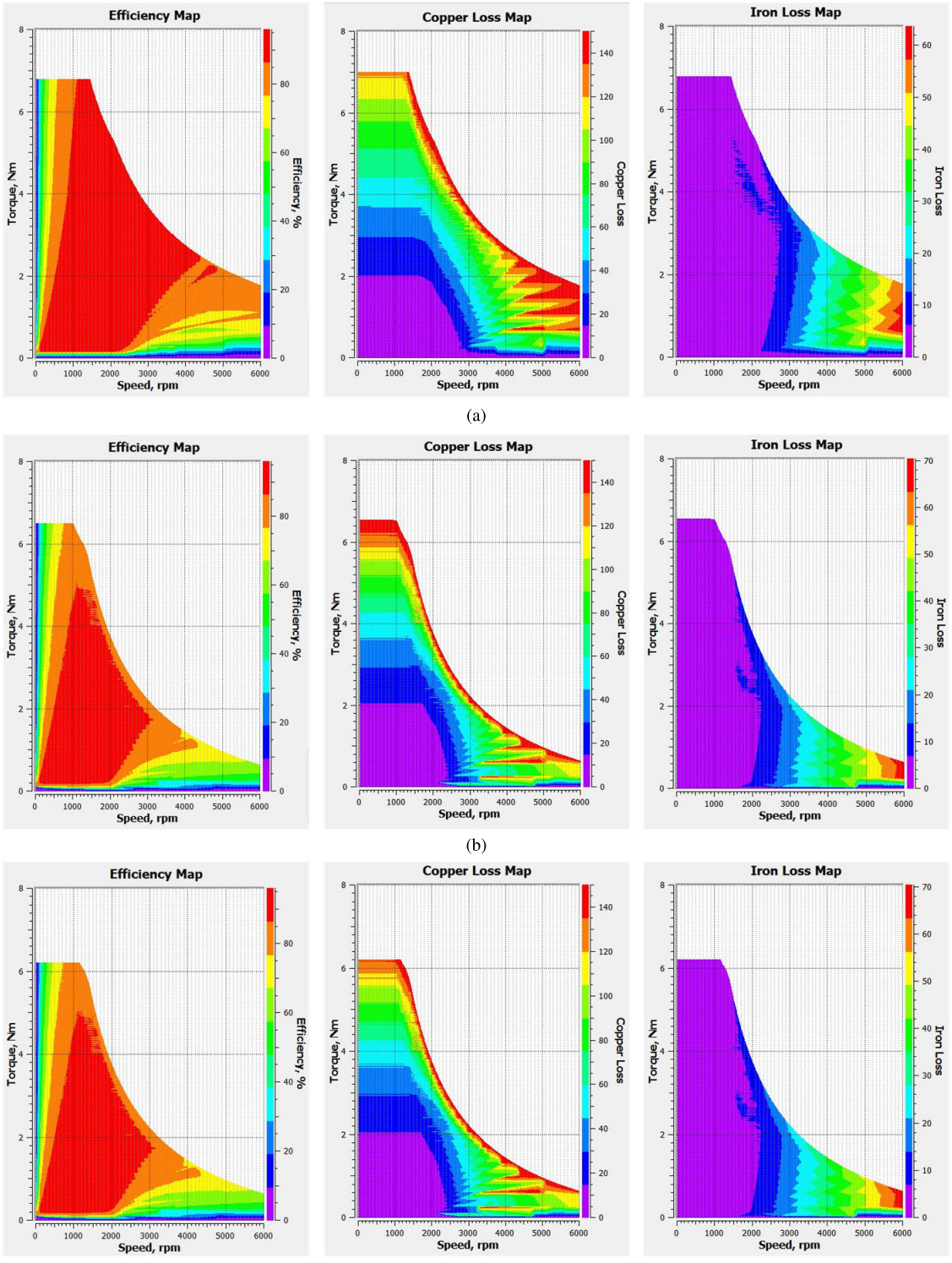

FIGURE 14. Efficiency and losses comparison at a rated current 10A, 120V U_{dc}. (a) AIPM-P, (b) AIPM-I, and (c) AIPM-II.

Three alternative topologies of instantaneous torque waveforms under maximum torque conditions are compared in Fig. 10, in which the instantaneous torque of the proposed design AIPM-P is higher than the conventional designs. The torque ripples of the AIPM-P are less compared to the AIPM-I and AIPM-II which is advantageous for the proposed AIPM-P. In order to get the torque ripple factors, the peak-to-peak torque fluctuation amplitudes are divided by the mean

TABLE 4. Losses comparison of the proposed design with conventional designs.

Parameter	AIPM-P	AIPM-I	AIPM-II
Iron losses (W)	34.055	35.84548	38.27541
Copper losses (W)	138		
PM losses (W)	0.205778	0.164526	0.227992
Average torque (Nm)	6.78	6.5	6.21
Efficiency (%)	95.41	94	94

torque value. The average torques of the presented topologies are compared in Fig. 11 across a broad range of current amplitudes up to 100A, confirming that the AIPM consistently has the higher torque, proceeded by AIPM-I and AIPM-II, regardless of the load level (light, rated, or overloaded). Fig. 12 shows the comparison of the loaded magnetic flux density and flux distribution of the presented topologies.

C. CONSTANT POWER SPEED RANGE (CPSR)

The CPSR performance of machines is crucial for variable-speed applications with a broad speed range. The torque versus speed and power versus speed wave shape of the proposed and the two conventional machines are generated using the method presented in [8] and [9] at rated current ($I_{max} = 10A$), DC voltage (120 V), and the maximum speed given to the motor is 6000 rpm. Fig. 13 shows the comparison of the CSPR performances of different topologies.

As shown, all three topologies are capable of operating at high speeds, but the proposed AIPM-P design has a superior CPSR performance due to the enhancement of average torque. The proposed AIPM-P topology exhibit good CPSR performances throughout a large speed range, however, when operating speeds are increased, the considerable torque improvement in the persistent torque zone rapidly decreases in the persistent power zone.

D. COMPARISON OF EFFICIENCY AND LOSSES MAPS

The efficiency and losses (copper and iron losses) maps of the three models at a rated current ($I_{max} = 10A$) and DC voltage (120 V) are compared, shown in Fig. 14 and tabulated in Table 4. The efficiency of the proposed design AIPM-P is higher than the other two conventional designs at low-speed (1500 rpm) and high-speed (>1500 rpm) regions. The proposed design AIPM-P has 95.41% efficiency, which is greater than the efficiency (94%) of the conventional AIPM-I and AIPM-II.

The copper and iron losses of the three designs are shown in Fig. 14. The copper losses at high torque conditions are greater than the lower torque conditions, while the iron losses at high torque conditions are lower than the high torque conditions because the copper losses depend on the stator current while the iron losses depend on the speed of the motor. Fig. 14 clearly shows that the iron losses at low speeds are lower than the high speed of the three designs, also the proposed design AIPM-P has lower iron losses than the conventional designs. The copper losses of the proposed model and the conventional designs AIPM-I and AIPM-II at high torque conditions.

IV. CONCLUSION

A novel AIPM-P synchronous machine for electric vehicles was proposed and analyzed. In the proposed AIPM-P, the conventional V-shape PM design is replaced with delta-shape magnets while keeping the same volume of PMs. The magnetic-field-shifting effect helped get the peak point of T_{PM} and T_r components closer, and the current advancing angle difference decreased; thus, the total average torque increased. The key electromagnetic performances of the proposed and the conventional machines were investigated by using the finite element method and compared. Finally, comparing the efficiency maps and losses analysis of all three designs, the proposed design clearly shows better efficiency of 95.41% while the conventional designs have 94%.

REFERENCES

[1] K. T. Chau, C. C. Chan, and C. Liu, "Overview of permanent-magnet brushless drives for electric and hybrid electric vehicles," *IEEE Trans. Ind. Electron.*, vol. 55, no. 6, pp. 2246–2257, Jun. 2008.

[2] Q. Ma, A. El-Refaie, and B. Lequesne, "Low-cost interior permanent magnet machine with multiple magnet types," *IEEE Trans. Ind. Appl.*, vol. 56, no. 2, pp. 1452–1463, Mar. 2020.

[3] I. Boldea, L. N. Tutelea, L. Parsa, and D. Dorrell, "Automotive electric propulsion systems with reduced or no permanent magnets: An overview," *IEEE Trans. Ind. Electron.*, vol. 61, no. 10, pp. 5696–5711, Oct. 2014.

[4] H. Cai, B. Guan, and L. Xu, "Low-cost ferrite PM-assisted synchronous reluctance machine for electric vehicles," *IEEE Trans. Ind. Electron.*, vol. 61, no. 10, pp. 5741–5748, Oct. 2014.

[5] L. Nicoletti, A. Romano, A. König, P. Köhler, M. Heinrich, and M. Lienkamp, "An estimation of the lightweight potential of battery electric vehicles," *Energies*, vol. 14, no. 15, p. 4655, Jul. 2021.

[6] I. Aghabali, J. Bauman, P. J. Kollmeyer, Y. Wang, B. Bilgin, and A. Emadi, "800-V electric vehicle powertrains: Review and analysis of benefits, challenges, and future trends," *IEEE Trans. Transport. Electrific.*, vol. 7, no. 3, pp. 927–948, Sep. 2021.

[7] S. Nategh, A. Boglietti, Y. Liu, D. Barber, R. Brammer, D. Lindberg, and O. Aglen, "A review on different aspects of traction motor design for railway applications," *IEEE Trans. Ind. Appl.*, vol. 56, no. 3, pp. 2148–2157, May 2020.

[8] M. Du, Y. Tian, W. Wang, Z. Ouyang, and K. Wei, "A novel finite-control-set model predictive directive torque control strategy of permanent magnet synchronous motor with extended output," *Electronics*, vol. 8, no. 4, p. 388, Mar. 2019.

[9] Y. Yang, S. M. Castano, R. Yang, M. Kasprzak, B. Bilgin, A. Sathyan, H. Dadkhah, and A. Emadi, "Design and comparison of interior permanent magnet motor topologies for traction applications," *IEEE Trans. Transport. Electrific.*, vol. 3, no. 1, pp. 86–97, Mar. 2017.

[10] N. Baloch, S. Atiq, and B.-I. Kwon, "A wound-field pole-changing Vernier machine for electric vehicles," *IEEE Access*, vol. 8, pp. 91865–91875, 2020.

[11] R. H. Staunton, T. A. Burress, and L. D. Marlino, "Evaluation of 2005 Honda accord hybrid electric drive system," Oak Ridge Nat. Lab. (ORNL), Oak Ridge, TN, USA, Tech. Rep. ORNL/TM-2006/535, Sep. 2006.

[12] K. Kamiev, J. Montonen, M. P. Ragavendra, J. Pyrhönen, J. A. Tapia, and M. Niemela, "Design principles of permanent magnet synchronous machines for parallel hybrid or traction applications," *IEEE Trans. Ind. Electron.*, vol. 60, no. 11, pp. 4881–4890, Nov. 2013.

[13] Y. Xiao, Z. Q. Zhu, G. W. Jewell, J. T. Chen, D. Wu, and L. M. Gong, "A novel asymmetric interior permanent magnet synchronous machine," *IEEE Trans. Ind. Appl.*, vol. 58, no. 3, pp. 3370–3382, May 2022.

[14] S. Zhu, W. Chen, M. Xie, C. Liu, and K. Wang, "Electromagnetic performance comparison of multi-layered interior permanent magnet machines for EV traction applications," *IEEE Trans. Magn.*, vol. 54, no. 11, pp. 1–5, Nov. 2018.

[15] A. M. El-Refaie, J. P. Alexander, S. Galioto, P. B. Reddy, K.-K. Huh, P. de Bock, and X. Shen, "Advanced high-power-density interior permanent magnet motor for traction applications," *IEEE Trans. Ind. Appl.*, vol. 50, no. 5, pp. 3235–3248, Sep. 2014.
[16] X. Liu, H. Chen, J. Zhao, and A. Belahcen, "Research on the performances and parameters of interior PMSM used for electric vehicles," *IEEE Trans. Ind. Electron.*, vol. 63, no. 6, pp. 3533–3545, Jun. 2016.
[17] X. Chen, J. Wang, V. I. Patel, and P. Lazari, "A nine-phase 18-slot 14-pole interior permanent magnet machine with low space harmonics for electric vehicle applications," *IEEE Trans. Energy Convers.*, vol. 31, no. 3, pp. 860–871, Sep. 2016.
[18] S. S. Maroufian and P. Pillay, "Design and analysis of a novel PM-assisted synchronous reluctance machine topology with AlNiCo magnets," *IEEE Trans. Ind. Appl.*, vol. 55, no. 5, pp. 4733–4742, Sep. 2019.
[19] A. Fatemi, D. M. Ionel, M. Popescu, Y. C. Chong, and N. A. O. Demerdash, "Design optimization of a high torque density spoke-type PM motor for a formula e race drive cycle," *IEEE Trans. Ind. Appl.*, vol. 54, no. 5, pp. 4343–4354, Sep. 2018.
[20] E. Carraro, N. Bianchi, S. Zhang, and M. Koch, "Design and performance comparison of fractional slot concentrated winding spoke type synchronous motors with different slot-pole combinations," *IEEE Trans. Ind. Appl.*, vol. 54, no. 3, pp. 2276–2284, May 2018.
[21] W. Zhao, F. Zhao, T. A. Lipo, and B. Kwon, "Optimal design of a novel V-type interior permanent magnet motor with assisted barriers for the improvement of torque characteristics," *IEEE Trans. Magn.*, vol. 50, no. 11, pp. 1–4, Nov. 2014.
[22] Y. Xiao, Z. Q. Zhu, S. S. Wang, G. W. Jewell, J. T. Chen, D. Wu, and L. M. Gong, "A novel asymmetric interior permanent magnet machine for electric vehicles," *IEEE Trans. Energy Convers.*, vol. 36, no. 3, pp. 2404–2415, Sep. 2021.
[23] Z. Zhu and Y. Xiao, "Novel magnetic-field-shifting techniques in asymmetric rotor pole interior PM machines with enhanced torque density," *IEEE Trans. Magn.*, vol. 58, no. 2, pp. 1–10, Feb. 2022.
[24] R. Dutta, A. Pouramin, and M. F. Rahman, "A novel rotor topology for high-performance fractional slot concentrated winding interior permanent magnet machine," *IEEE Trans. Energy Convers.*, vol. 36, no. 2, pp. 658–670, Jun. 2021.
[25] W. Zhao, F. Xing, X. Wang, T. A. Lipo, and B. Kwon, "Design and analysis of a novel PM-assisted synchronous reluctance machine with axially integrated magnets by the finite-element method," *IEEE Trans. Magn.*, vol. 53, no. 6, pp. 1–4, Jun. 2017.
[26] Y. Xiao, Z. Q. Zhu, G. W. Jewell, J. Chen, D. Wu, and L. Gong, "A novel asymmetric rotor interior permanent magnet machine with hybrid-layer permanent magnets," *IEEE Trans. Ind. Appl.*, vol. 57, no. 6, pp. 5993–6006, Nov. 2021.
[27] Y. Xiao, Z. Q. Zhu, G. W. Jewell, J. Chen, D. Wu, and L. Gong, "A novel spoke-type asymmetric rotor interior permanent magnet machine," *IEEE Trans. Ind. Appl.*, vol. 57, no. 5, pp. 4840–4851, Sep. 2021.
[28] X. Sun, Z. Shi, Y. Cai, G. Lei, Y. Guo, and J. Zhu, "Driving-cycle-oriented design optimization of a permanent magnet hub motor drive system for a four-wheel-drive electric vehicle," *IEEE Trans. Transport. Electrific.*, vol. 6, no. 3, pp. 1115–1125, Sep. 2020.
[29] X. Sun, N. Xu, and M. Yao, "Sequential subspace optimization design of a dual three-phase permanent magnet synchronous hub motor based on NSGA III," *IEEE Trans. Transport. Electrific.*, vol. 9, no. 1, pp. 622–630, Mar. 2023.
[30] Z. Shi, X. Sun, Y. Cai, and Z. Yang, "Robust design optimization of a five-phase PM hub motor for fault-tolerant operation based on Taguchi method," *IEEE Trans. Energy Convers.*, vol. 35, no. 4, pp. 2036–2044, Dec. 2020.

NIAZ MUHAMMAD received the B.S. degree in electronics engineering from the University of Engineering and Technology, Peshawar, Pakistan, in 2020. He is currently pursuing the M.S. degree in electrical engineering from COMSATS University Islamabad, Abbottabad Campus. His research interests include design, optimization, and the analysis of interior permanent magnet machines.

FAISAL KHAN (Senior Member, IEEE) received the B.S. degree in electronics engineering and the M.S. degree in electrical engineering from COMSATS University Islamabad, Abbottabad Campus, Pakistan, in 2009 and 2012, respectively, and the Ph.D. degree in electrical engineering from Universiti Tun Hussein Onn Malaysia, Malaysia, in 2017. From 2010 to 2012, he was a Lecturer with the University of Engineering and Technology, Peshawar, Abbottabad Campus. Since 2017, he has been an Assistant Professor with the Department of Electrical Engineering, COMSATS University Islamabad. He is the author of more than 170 publications and two patents. His research interests include the design of flux-switching, synchronous, and DC machines. Furthermore, he is a member of IEEE Industrial Electronics Society and IEEE-IES Electrical Machines Technical Committee. He has received multiple research awards.

BASHARAT ULLAH (Member, IEEE) received the B.S. degree in electronics engineering from the University of Engineering and Technology, Peshawar, Pakistan, in 2015, the M.S. degree in electrical engineering from the National University of Sciences and Technology, Islamabad, Pakistan, in 2017, and the Ph.D. degree in electrical engineering from COMSATS University Islamabad, Abbottabad Campus, in 2023. Since 2019, he has been a Research Associate with the Research in Design of Electric Machines (RiDEM) Laboratory. This Laboratory is part of the Department of Electrical and Computer Engineering, COMSATS University Islamabad, Abbottabad Campus, Abbottabad, Pakistan. His research interests include the design, optimization and analysis of rotary and linear hybrid excited flux-switching machines, linear actuators, and polyphase machines and their drives. Furthermore, he is a member of the IEEE-IES Electrical Machines Technical Committee.

SAIRA TARIQ received the B.S. degree in electrical (power) engineering from COMSATS University Islamabad, Abbottabad Campus, Pakistan, in 2021, where she is currently pursuing the M.S. degree in electrical engineering. Her research interests include the design and analysis of linear machines and interior permanent magnet machines.

AHMAD H. MILYANI received the B.Sc. (Hons.) and M.Sc. degrees in electrical and computer engineering from Purdue University, in 2011 and 2013, respectively, and the Ph.D. degree in electrical engineering from the University of Washington, in 2019. He is currently an Assistant Professor with the Department of Electrical and Computer Engineering, King Abdulaziz University, Jeddah, Saudi Arabia. His research interests include power systems operation and optimization, renewable and sustainable energy, power electronics, electric machines, electric vehicles, and machine learning.